Warsaw University of Technology
Faculty of Physics

Master's diploma thesis

in the field of study Applied Physics
and specialisation

Quantum vortices in two-dimensional ultracold atomic gases

thesis number according to Faculty's thesis evidence: {number}

Mateusz Ślusarczyk

student record book number: 311842

supervisor:
dr Marek Tylutki

second supervisor:
dr hab. Krzysztof Pawłowski

WARSAW 2025

Abstract

Thesis title: Quantum vortices in two-dimensional ultracold atomic gases

Quantum vortices play a central role in the two-dimensional physics of ultracold gases and are typically well-described within the mean-field framework. In this thesis, we investigate the emergence of vortices in the eigenstates of the N-body Hamiltonian for interacting bosons confined to a disk. Our approach is inspired by earlier studies connecting solitons to yrast states in one-dimensional systems. The analysis is based on conditional states obtained by sequentially measuring particle positions, revealing both the density and phase profiles characteristic of a quantum vortex—albeit with quantum fluctuations in the vortex core position. This many-body perspective is further supported by a Bogoliubov analysis, providing insight into condensate depletion and excitation modes.

Keywords
quantum vortices, ultracold gases

{supervisor's signature} {student's signature}

Streszczenie

Tytuł pracy: Kwantowe wiry w dwuwymiarowych ultrazimnych gazach atomowych

Wir kwantowy odgrywa kluczową rolę w dwuwymiarowej fizyce ultrazimnych gazów i zazwyczaj jest dobrze opisywany w przybliżeniu średniego pola. W niniejszej pracy badamy pojawianie się wirów w stanach własnych hamiltonianu układu N oddziałujących bozonów, ograniczonych do dysku. Nasze podejście inspirowane jest wcześniejszymi badaniami łączącymi solitony ze stanami yrast w układach jednowymiarowych. Analiza opiera się na stanach warunkowych, uzyskanych poprzez sekwencyjny pomiar położeń cząstek, które ujawniają zarówno rozkład gęstości, jak i fazy typowy dla wiru kwantowego — jednak z uwzględnieniem fluktuacji kwantowych położenia rdzenia wiru. To podejście wielu ciał uzupełnione jest analizą metodą Bogoliubova, dostarczając informacji o ubytku kondensatu oraz o modach wzbudzeń.

Słowa kluczowe:
wiry kwantowe, ultrazimne gazy

{podpis opiekuna naukowego} {podpis studenta}

Contents

1 Introduction **9**

2 Theory **13**

2.1 Many body problem 14

2.2 Solitons 15

2.3 Quantum vortices 17

3 Model **19**

3.1 Many-body problem 20

3.2 Interaction 23

3.3 Bogoliubov-de Gennes 24

4 Numerical methods **27**

4.1 Exact diagonalization 28

4.2 Particles drawing 31

4.3 Mean field and Bogoliubov-de Gennes 32

4.4 Technical details 34

5 Results **35**

5.1 Quntities 36

5.2 Vortex in the many body wave function 39

6 Conclusions **43**

A Interaction integral **53**

Chapter 1

Introduction

Describing quantum systems using the fundamental many-body Schrödinger equation is often too complex, impractical, or even impossible. As a result, simpler methods—particularly mean-field approaches—have been employed to study systems of interacting particles. These methods have successfully captured a variety of phenomena. For instance, in one-dimensional systems of interacting bosons, one can study dark solitons: localized dips in density that travel uniformly through the bulk. These are solutions to the nonlinear, time-dependent mean-field Gross-Pitaevskii equation.

However, in principle, such solitonic behavior should also be describable within the framework of the linear many-body Schrödinger equation. This is exemplified by the Lieb-Liniger model, which describes a one-dimensional gas of bosons with periodic boundary conditions and delta-function interactions. This model has been solved analytically [1, 2], and certain classes of its solutions bear resemblance to dark solitons [3]. The potential connection between these solutions and solitons has inspired further investigations [4, 5], which revealed that solitons emerge from many-body solutions through a mechanism of symmetry breaking—specifically, by "measuring" a subset of particle positions.

The main goal of this thesis is to further explore how structures known from mean-field theory emerge in exact many-body solutions. Our focus shifts from solitons to quantized vortices, topological defects that are well-understood within the mean-field framework.

Quantized vortices play a crucial role in various phenomena observed in superfluids, in particular in ultracold atoms – the system we focus on in this master thesis. In two-dimensional systems, vortices form lattice structures [6] or participate in phase transitions such as the Berezinskii-Kosterlitz-Thouless transition [7, 8, 9], where the system shifts from bound vortex-antivortex pairs at low temperatures to unbound defects above a critical temperature. In three dimensions, vortices appear as vortex lines around which superfluid rotation occurs, leading to phenomena like quantum turbulence [10], where tangled vortex lines resemble a complex web. These patterns offer insights into decay mechanisms and hydrodynamic behavior in atomic gases.

To study vortices in a many-body setting, we adopt a similar strategy to that used for solitons. We model a two-dimensional gas of interacting bosons with short-range interactions, represented by a narrow Gaussian potential. The atoms are confined to a disk-shaped trap (see Figure 1.1), which ensures conservation of total angular momentum. This allows us to focus on a class of excited states with the lowest energy for a given angular momentum—known as yrast states. Unlike the one-dimensional case with delta-function interactions, no analytical solutions exist in this setup, so we rely on numerical methods. We solve the many-body problem via exact diagonalization with importance truncation [11].

To reveal vortex structures, we again use symmetry breaking through the "measurement" of particles positions in the yrast state. We find that vortices emerge at random locations away from the center of the disk, yet they exhibit dynamical stability. This stability is confirmed by evolving the system using the time-dependent mean-field equations.

In Chapter 2, we begin with an overview of both many-body and mean-field approaches for interacting bosons. We also review how solitons have been identified in 1D many-body systems and introduce the concept of quantum vortices within the Gross-Pitaevskii framework. Chapter 3 presents our two-dimensional model and the theoretical tools used for its analysis. Chapter 4 outlines the computational methods, with particular emphasis on importance truncation in exact diagonalization. Our main findings are presented in Chapter 5, followed by concluding remarks in Chapter 6.

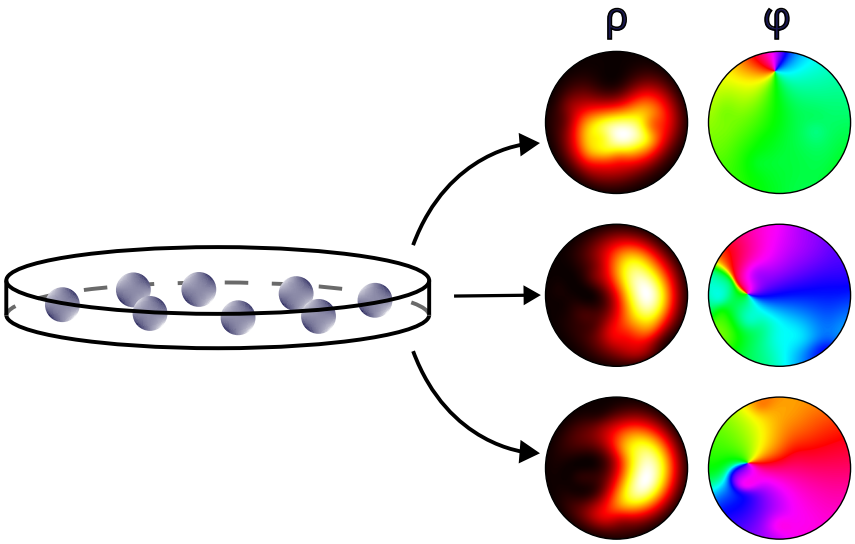

Figure 1.1: Abstract

Chapter 2

Theory

This chapter provides a brief overview of the quantum mechanical N-body problem for interacting indistinguishable particles, specifically bosons, and introduces the Gross–Pitaevskii equation. We explain the concept of solitons and how they emerge from many-body solutions. Before turning to quantum vortices, we introduce the notion of the conditional wave function—a key tool in which vortices will later be identified.

2.1 Many body problem

In the quantum mechanics, the state of an N-particle system if fully characterized by its N-particle wave function

$$\Psi = \Psi(\boldsymbol{r}_1, \dots, \boldsymbol{r}_N, t), \tag{2.1}$$

where $|\Psi(\boldsymbol{r}_1, \dots, \boldsymbol{r}_N, t)|^2$ is the probability density of finding the first particle at $\boldsymbol{r}_1$, the second at $\boldsymbol{r}_2$, and so on, at time t. The time dependence of the wave function is governed by the time-dependent Schrödinger equation

$$i\hbar \frac{\partial}{\partial t} \Psi(\boldsymbol{r}_1, \dots, \boldsymbol{r}_N, t) = \hat{H} \Psi(\boldsymbol{r}_1, \dots, \boldsymbol{r}_N, t), \tag{2.2}$$

where $\hat{H}$ is the Hamiltonian operator. In this work, we restrict ourselves to Hamiltonians of the form

$$\hat{H} = \sum_{i=1}^{N} \left(-\frac{\hbar^2}{2m} \nabla_i^2 + V_{\mathrm{ex}}(\boldsymbol{r}_i) \right) + \frac{1}{2} \sum_{i \neq j} V(|\boldsymbol{r}_i - \boldsymbol{r}_j|), \tag{2.3}$$

where $V_{\mathrm{ex}}(\boldsymbol{r})$ is an external potential, and $V(r)$ is an interaction potential that depends only on the distance between the particles. For indistinguishable particles the probabilities should be independent of the permutation of particles. Moreover, exchanging two particle positions $\boldsymbol{r}_i$ and $\boldsymbol{r}_j$ twice must leave the wave function unchanged. This implies that the wave function must transform under particle exchange according to

$$\Psi(\dots, \boldsymbol{r}_i, \dots, \boldsymbol{r}_j, \dots) = \pm \Psi(\dots, \boldsymbol{r}_j, \dots, \boldsymbol{r}_i, \dots). \tag{2.4}$$

Particles whose wave function are symmetric (with the plus sign) are called bosons, while those with antisymmetric wave functions (minus sign) are fermions. In this thesis we focus on bosons. A primary method for understanding such systems is through their stationary states, described by the time independent Schrödinger equation

$$\hat{H} \Psi(\boldsymbol{r}_1, \dots, \boldsymbol{r}_N, t) = E \Psi(\boldsymbol{r}_1, \dots, \boldsymbol{r}_N, t), \tag{2.5}$$

where E is the total energy of the system.

The full N-particle wave function Ψ is generally difficult to analyze directly. One useful quantity that provides insight is the single particle density matrix (SPDM)

$$\rho(\boldsymbol{r}, \boldsymbol{r}') = N \int \Psi^*(\boldsymbol{r}', \boldsymbol{r}_2, \dots, \boldsymbol{r}_N) \Psi(\boldsymbol{r}, \boldsymbol{r}_2, \dots, \boldsymbol{r}_N) \, \mathrm{d}\boldsymbol{r}_2 \cdots \mathrm{d}\boldsymbol{r}_N, \tag{2.6}$$

whose diagonal

$$\rho(\boldsymbol{r}) = \rho(\boldsymbol{r}, \boldsymbol{r}) \tag{2.7}$$

gives the average particle density at position $\boldsymbol{r}$.

Directly solving Eq. (2.5) is difficult or impractical task, or in many cases even impossible and one has to employ different methods of approximation. For the symmetric wave function of bosons, one of the simplest approaches is to postulate the form of a wave function as if all the particles were lying in the same single-particle state $\phi(\boldsymbol{r})$ and the wave function is then given by the product

$$\Psi_{\mathrm{GP}}(\boldsymbol{r}_1, \ldots, \boldsymbol{r}_N) = \prod_{i=1}^{N} \phi(\boldsymbol{r}_i). \tag{2.8}$$

When we calculate the energy of a state described by the wavefunction given in the form Ψ_{GP}, that is $\langle \Psi_{\mathrm{GP}} | \hat{H} | \Psi_{\mathrm{GP}} \rangle$, we obtain the energy functional dependent on the ϕ in the form

$$E[\phi] = N \int \phi^* \left(-\frac{\hbar^2}{2m} \nabla^2 \right) \phi \, \mathrm{d}\boldsymbol{r} + \frac{1}{2} N(N-1) \iint |\phi(\boldsymbol{r})|^2 V(|\boldsymbol{r} - \boldsymbol{r}'|) |\phi(\boldsymbol{r}')|^2 \, \mathrm{d}\boldsymbol{r} \, \mathrm{d}\boldsymbol{r}'. \tag{2.9}$$

One can minimize this functional with the constraint on the normalization $\int |\phi|^2 = 1$, using the Lagrange multiplier $N\mu$. Then, the variation $\delta(E - N\mu \int |\phi|^2) = 0$ with respect to ϕ^* yields the equation

$$\left(-\frac{\hbar^2}{2m} \nabla^2 + V_{\mathrm{ex}}(\boldsymbol{r}) + V_{\mathrm{MF}}(\boldsymbol{r}) \right) \phi(\boldsymbol{r}) = \mu \phi(\boldsymbol{r}), \tag{2.10}$$

where we introduce the mean-field potential

$$V_{\mathrm{MF}}(\boldsymbol{r}) = (N-1) \int V(|\boldsymbol{r} - \boldsymbol{r}'|) |\phi(\boldsymbol{r}')|^2 \, \mathrm{d}\boldsymbol{r}'. \tag{2.11}$$

The quantity μ is called the chemical potential. The Eq. (2.10) is known as the time independent Gross-Pitaevskii equation, which we marked using the subscript GP in Eq. (2.8). Although above equation looks very similar to the Schrödinger equation, it is nonlinear as can be seen from the mean-field potential which is dependent on ϕ. Energy can be calculated from Eq. (2.9) (note that $E[\phi] \neq \mu$), while the density of particles is simply given by $N|\phi(\boldsymbol{r})|$.

Mean-field can also be used in the time dependent case, where one uses the time-dependent principle of least action [12] to obtained the equation of motion, namely the time dependent Gross-Pitaevskii equation

$$i\hbar \frac{\partial}{\partial t} \phi(\boldsymbol{r}, t) = \left(-\frac{\hbar^2}{2m} \nabla^2 + V_{\mathrm{ex}}(\boldsymbol{r}) + V_{\mathrm{MF}}(\boldsymbol{r}, t) \right) \phi(\boldsymbol{r}, t). \tag{2.12}$$

We will be considering the N-body problem using the Hamiltonian in (2.3), and examine the connection between its excited states eigenstates and the solutions of the time-dependent mean-field equation (2.12). This relationship has previously been explored in the context of solitons, which are localized excitations in one-dimensional systems.

2.2 Solitons

One of the simplest exactly solvable models of interacting quantum particles is the Lieb-Liniger model [1, 2], which describes a one-dimensional system of bosons with periodic boundary conditions. The interaction potential is given by $V(x) = g\delta(x)$, where the parameter g controls the

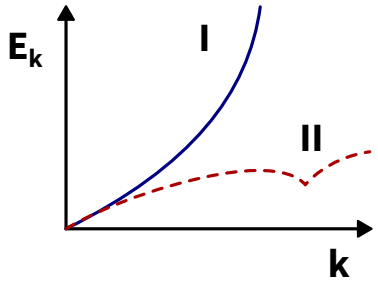

Figure 2.1: Scheme showing energies of type I and type II excitations [2, 1] as functions of the momentum k.

interaction strength. The corresponding Hamiltonian takes the form

$$\hat{H}_{\mathrm{LL}} = -\frac{\hbar^2}{2m}\sum_{i=1}^{N}\frac{\partial^2}{\partial x^2} + \frac{g}{2}\sum_{i\neq j}\delta(|x_i - x_j|). \tag{2.13}$$

This model admits an exact analytical solution via the Bethe ansatz, which reduces the problem of finding eigenstates to solving a set of transcendental equations. The eigenstates are labeled by a set $\{I_k\}_{k=1}^{N}$ with I_j being integers if N is odd, or half-integers for even N. The ground state is obtained by choosing a consecutive set centered around zero: $\{I_k\} = \{-(N-1)/2, -(N-1)/2+1, \ldots .(N-1)/2\}$.

Excitations of the system can be generated by modifying these quantum numbers. In particular, type I excitations arise by increasing the magnitude of the outermost quantum number—these excitations correspond to the Bogoliubov spectrum. On the other hand, type II excitations, also known as one-hole excitations, involve removing an I_k from within the ground state configuration and placing it just outside the contiguous band, such as at $-(N-1)/2-1$ or $(N-1)/2+1$. Sketches of both excitation spectra are shown in Fig. 2.1.

While type I excitations were immediately identified with the Bogoliubov spectrum, it was only years later that type II excitations were found to be related to dark solitons, through a comparison of their dispersion relations [3]. A dark soliton is nonlinear, localized excitation known from mean-field theory, where it appears as a solutions to the time-dependent Gross-Pitaevskii equation. In the case of δ-type interaction, the equation takes on a particularly simple form

$$i\hbar\frac{\partial}{\partial t}\phi(x,t) = \left(-\frac{\hbar^2}{2m}\frac{\partial^2}{\partial x^2} + g(N-1)|\phi(x,t)|^2\right)\phi(x,t). \tag{2.14}$$

Dark solitons are characterized by a local dip in density that propagates without dispersion, accompanied by a rapid phase shift. When the density at the center of the dip vanishes entirely, the soliton is termed black; otherwise it is referred to as a gray soliton. (see Fig. 2.2).

However, identifying soliton-like features in the exact many-body eigenstates of the Lieb-Liniger model is nontrivial. Due to translational invariance, the diagonal of the single-particle density matrix $\rho(x)$ is uniform, and so no features are visible. Moreover, direct access to the phase profile is not possible from $\rho(x)$ alone.

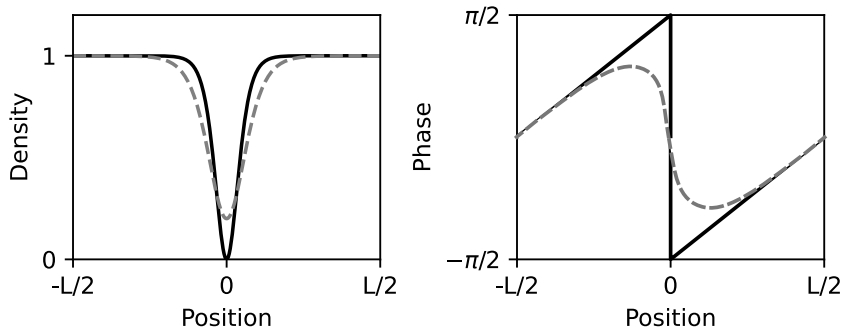

Figure 2.2: Examples of a black soliton (black solid line) and a grey soliton (grey dashed line). The left panel shows the density profile, while the right panel displays the phase of the macroscopic orbital. A characteristic feature of solitons is the sharp phase variation at their center; in the case of the black soliton, this manifests as a phase jump of π, indicating a discontinuity.

An approach to solve this issue was performed in [4], where the authors used the concept of a conditional wave function, defined as

$$\psi_{\text{cond}}(x) = \psi(\bar{x}_1, \bar{x}_2, \ldots, \bar{x}_{N-1}, x), \tag{2.15}$$

in which $\bar{x}_1, \ldots, \bar{x}_{N-1}$ are fixed particle positions obtained by sequential measurements. This effectively reduces the many-body wave function to a single-particle function of x, allowing one to probe its spatial and phase structure. A more detailed description of this measurement procedure is provided in the next chapter.

When applied to type II excitations of the Lieb-Liniger model, this conditional wave function reveals both the density depletion and phase jump characteristic of a dark soliton. This approach has also been extended to investigate soliton dynamics [13] and soliton-like features in the non-interacting limit [14].

Solutions to the N-body problem have been shown to correspond to one-dimensional objects known as solitons. This type of analysis can be naturally extended to two dimensions, where the counterparts of solitons are quantum vortices. The investigation of this correspondence forms the central focus of this thesis.

2.3 Quantum vortices

An important structure that arises in two dimensions is the quantum vortex, which will be the primary focus of this thesis. The main objective is to identify vortices within the many-body wave function using the same approach employed in the soliton case—namely, the analysis of the conditional wave function.

Quantum vortex could be explained in the mean-field framework, where one considers the macroscopic orbital $\phi(\boldsymbol{r}, t)$, a complex-valued function that can be decomposed into two real-valued functions as

$$\phi(\boldsymbol{r}, t) = \sqrt{n(\boldsymbol{r}, t)} e^{i\theta(\boldsymbol{r}, t)}, \tag{2.16}$$

where $n(\boldsymbol{r}, t) \geq 0$ represents the density and $\theta(\boldsymbol{r}, t)$ is the phase.

To understand the notion of a vortex, consider the phase function θ, a starting point $\boldsymbol{r}$, and a closed path Γ that loops around and returns to $\boldsymbol{r}$ (see Fig. 2.3). Since ϕ is single-valued, its phase must change by an integer multiple of 2π upon completing the loop. Mathematically, this is expressed as:

$$\int_{\Gamma} \nabla(\theta) \cdot \mathrm{d}\boldsymbol{l} = 2\pi q, \tag{2.17}$$

where $q \in \mathbb{Z}$. A point around which this phase winding is nonzero ($q \neq 0$) is identified as the vortex core, and q is referred to as the vortex charge.

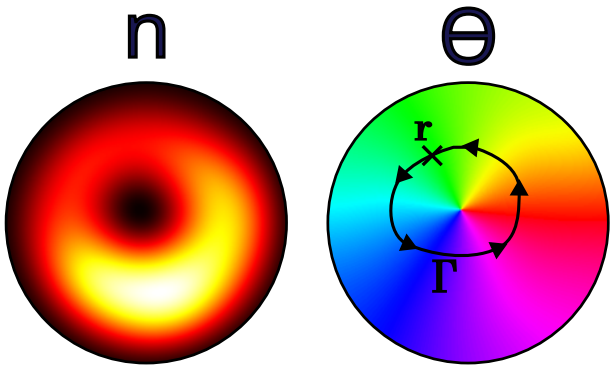

Figure 2.3: Left: density n, and right: phase θ, of a quantized vortex in the mean-field orbital ϕ. In the core of the vortex the density drops to zero and the phase changes around that point by 2π.

At the vortex core, the density n drops to zero, while the phase θ changes rapidly in its vicinity. In practice, for infinitesimally small loops, q typically takes the values -1, 0, or 1, as it is energetically more favorable—due to interactions—for the system to support multiple vortices with the lowest possible charge rather than a single vortex with higher charge.

The subsequent chapters will address the challenge of detecting vortices in the many-body wave function, guided by the insights provided by mean-field theory.

Chapter 3

Model

This chapter is devoted to formulating the model of the system in which we search for vortices. We begin by introducing the second quantization formalism used to describe the many-body problem. Next, we present the model interaction potential chosen for the system and explain its key properties. The chapter concludes with a brief overview of the number-conserving Bogoliubov–de Gennes method, a many-body approach based on the assumption that most of the atoms occupy the mean-field orbital.

3.1 Many-body problem

In the one-dimensional case—particularly within the Lieb-Liniger model—an important conserved quantity is total momentum of the systems. Solitons have been associated with type II excitations, which can be understood as excitations where momentum is added to particles in the ground state and distributed uniformly across a few of them. Thus, momentum emerges as the key quantity of interest in this context.

In our investigation of vortices in two dimensions, a natural analogue to momentum is the total angular momentum of the system, and so we chose a model in which angular momentum is conserved. We consider a system of interacting particles confined to a disc of radius R—that is, particles in a two-dimensional plane subject to an external potential of the form:

$$V_{\text{ex}}(\boldsymbol{r}) = \begin{cases} 0 & \text{if } |\boldsymbol{r}| < R, \\ +\infty & \text{if } |\boldsymbol{r}| > R. \end{cases} \tag{3.1}$$

When considering a single particle in this system, the Schrödinger equation in polar coordinates takes the form:

$$-\frac{\hbar^2}{2m}\left(\frac{\partial^2}{\partial r^2} + \frac{1}{r}\frac{\partial}{\partial r} + \frac{1}{r^2}\frac{\partial^2}{\partial \theta^2}\right)\phi_i(r,\theta) = E_i\phi_i(r,\theta), \tag{3.2}$$

where r denotes the radial distance from the center of a disc and θ is the azimuthal angle.

The external potential (3.1) is implemented as a hard-wall boundary condition: $\phi_i(R,\theta) = 0$. Outside the disc (i.e., for $r > R$), the wave function vanishes $\phi(r,\theta) = 0$. The quantum number $i \geq 0$ indexes the eigenstates in order of increasing energy energy: $E_0 \leq E_1 \leq E_2 \leq \cdots$.

The solution of (3.2) are obtained via separation of variables and take the form:

$$\psi_i(\boldsymbol{r}) = f_i(r)e^{im_i\theta}, \tag{3.3}$$

where $m_i \in \mathbb{Z}$ is the angular momentum quantum number. The radial part of the wave function is given by the Bessel function of the first kind:

$$f_i(r) = A_i J_{m_i}\left(\alpha_i \frac{r}{R}\right), \tag{3.4}$$

where the normalization constant A_i is

$$A_i = \left|R\sqrt{\pi}J_{m_i+1}(\alpha_i)\right|^{-\frac{1}{2}}. \tag{3.5}$$

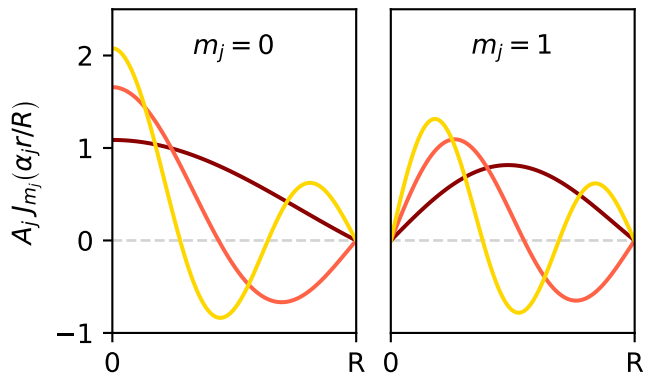

Figure 3.1: Radial part $f_i(r)$ of the single particle wave function. For the angular momentum $m\hbar$ those are given by the m-th Bessel functions of the first kind, rescaled by consecutive zeros of the Bessel function, so that $f_i(R) = 0$.

α_i is a positive real number corresponding to a zero of the m_i-th Bessel function. This ensures the boundary condition $f_i(R) = 0$ is satisfied. The correspond energy eigenvalue is:

$$E_i = \frac{\hbar^2 \alpha_i^2}{2mR^2}. \tag{3.6}$$

Examples of the radial functions $f_i(r)$ are shown in Fig. 3.1. While it is common to label these eigenstates with two quantum numbers—m, representing the angular momentum, and k, indicating the k-th zero of the m-th Bessel function—for clarity, we use a single index i to enumerate the states. Each i corresponds to a specific pair $(m_i,\ \alpha_i)$, where m_i denotes the angular momentum and α_i is a particular zero of J_{m_i}.

The system of interacting particles is described by the many-body Hamiltonian

$$\hat{H} = \sum_{i=1}^{N} \left(-\frac{\hbar^2}{2m} \nabla_i^2 + V_{\text{ex}}(\boldsymbol{r}_i) \right) + \frac{1}{2} \sum_{i \neq j} V(|\boldsymbol{r}_i - \boldsymbol{r}_j|), \tag{3.7}$$

and we have to solve the eigenproblem $\hat{H}\Psi = E\Psi$ finding the energies E and many body wave function $\Psi(\boldsymbol{r}_1, \ldots, \boldsymbol{r}_N)$.

In one dimension, and with a contact interaction modeled by a Dirac delta potential, analogous problem was solved analytically in the work of Lieb and Liniger [1, 2]. However, in two dimensions, exact solutions are generally not available, and numerical methods are required. In this context, it is convenient to reformulate the problem in the framework of second quantization, where the state of the system is described in the abstract Fock space, spanned by occupation number states $|\boldsymbol{n}\rangle$, with $\boldsymbol{n} = (n_0, n_1, n_2, \ldots)$.

Each integer $n_i \geq 0$ denotes the number of particles occupying the single-particle orbital ϕ_i, and the total number of particles is $\sum_i n_i = N$. A general quantum state in Fock space is a linear combination of theses occupation states:

$$|\Psi\rangle = \sum_{\boldsymbol{n}} C_{\boldsymbol{n}} |\boldsymbol{n}\rangle, \tag{3.8}$$

with the normalization condition $\sum |C_{\boldsymbol{n}}|^2 = 1$.

Since we are dealing with bosons, the wave function must be symmetric under particle exchange. The basis wave functions in the position-representation $\langle \boldsymbol{r}_1, \ldots, \boldsymbol{r}_N | \boldsymbol{n} \rangle$ can be expressed using the matrix permanent:

$$\langle \boldsymbol{r}_1, \ldots, \boldsymbol{r}_N | \boldsymbol{n} \rangle = \frac{1}{\sqrt{N! n_1! n_2! \ldots}} \operatorname{perm} \begin{pmatrix} \phi_{a_1}(\boldsymbol{r}_1) & \cdots & \phi_{a_N}(\boldsymbol{r}_1) \\ \vdots & \ddots & \vdots \\ \phi_{a_1}(\boldsymbol{r}_N) & \cdots & \phi_{a_N}(\boldsymbol{r}_N) \end{pmatrix}. \tag{3.9}$$

where the indices $a_1 \leq \cdots \leq a_N$ are the occupied orbitals, with each index repeated according to the number of particles in the corresponding orbital. The position-space representation of arbitrary state is then

$$\Psi(\boldsymbol{r}_1, \ldots, \boldsymbol{r}_N) = \langle \boldsymbol{r}_1, \ldots, \boldsymbol{r}_N | \Psi \rangle = \sum_{\boldsymbol{n}} C_{\boldsymbol{n}} \langle \boldsymbol{r}_1, \ldots, \boldsymbol{r}_N | \boldsymbol{n} \rangle. \tag{3.10}$$

We introduce the annihilation $\hat{a}_i$ and creation $\hat{a}_i^\dagger$ operators, which act on the states in the Fock space and satisfy the canonical bosonic commutation relations:

$$[\hat{a}_i, \hat{a}_j^\dagger] = \delta_{ij}, \quad [\hat{a}_i, \hat{a}_j] = [\hat{a}_i^\dagger, \hat{a}_j^\dagger] = 0. \tag{3.11}$$

Their action on an occupation number state $|n\rangle$ are given by:

$$\hat{a}_i | n_0, n_1, \ldots, n_i, \ldots \rangle = \sqrt{n_i} | n_0, n_1, \ldots, n_i - 1, \ldots \rangle, \tag{3.12}$$

$$\hat{a}_i^\dagger | n_0, n_1, \ldots, n_i, \ldots \rangle = \sqrt{n_i + 1} | n_0, n_1, \ldots, n_i + 1, \ldots \rangle. \tag{3.13}$$

Using these operators, the many-body Hamiltonian can be written in second quantized form as

$$\hat{H} = \sum_j E_j \hat{a}_j^\dagger \hat{a}_j + \frac{1}{2} \sum_{ijkl} V_{ijkl} \hat{a}_i^\dagger \hat{a}_j^\dagger \hat{a}_l \hat{a}_k, \tag{3.14}$$

where E_j are the single-particle energies defined in Eq. (3.6), and the interaction coefficients V_{ijkl} are given by the integrals

$$V_{ijkl} = \iint \phi_i^*(\boldsymbol{r}) \phi_j^*(\boldsymbol{r}') V(|\boldsymbol{r} - \boldsymbol{r}'|) \phi_k(\boldsymbol{r}') \phi_l(\boldsymbol{r}) \, \mathrm{d}\boldsymbol{r} \, \mathrm{d}\boldsymbol{r}'. \tag{3.15}$$

We also define the number operator $\hat{n}_i = \hat{a}_i^\dagger \hat{a}_i$, which counts the number of particles in orbital i. It satisfies $\hat{n}_i | \boldsymbol{n} \rangle = n_i | \boldsymbol{n} \rangle$. The total number of particles operator is then

$$\hat{N} = \sum_i \hat{n}_i. \tag{3.16}$$

It is straightforward to verify that $\hat{N}$ commutes with the Hamiltonian, i.e., $[\hat{H}, \hat{N}] = 0$, which expresses the particle number conservation. Therefore, when solving the eigenvalue problem

$$\hat{H} | \Psi \rangle = E | \Psi \rangle, \tag{3.17}$$

we can restrict our attention to the subspace with a fixed number of particles N. Further details regarding the numerical solution of Eq. (3.17) are presented in the chapter on numerical methods.

In addition to the energy, an important quantity characterizing a quantum many-body system is the particle density. We obtain it from the diagonal of the single particle density matrix (2.7). It is appropriate to use the field annihilation operator

$$\hat{\psi}(\boldsymbol{r}) = \sum_i \psi_i(\boldsymbol{r})\hat{a}_i \tag{3.18}$$

and its hermitian conjugate, the field creation operator

$$\hat{\psi}^\dagger(\boldsymbol{r}) = \sum_i \psi_i^*(\boldsymbol{r})\hat{a}_i^\dagger. \tag{3.19}$$

In the second-quantized formalism, the single-particle density matrix can then be written in the form:

$$\rho(\boldsymbol{r}, \boldsymbol{r}') = \left\langle \hat{\psi}^\dagger(\boldsymbol{r}')\hat{\psi}(\boldsymbol{r}) \right\rangle, \tag{3.20}$$

where the expectation value is taken with respect to the many-body state $|\Psi\rangle$. By expanding the field operator in a single particle basis $\{\phi_i\}$, we obtain a form suitable for numerical computation

$$\rho(\boldsymbol{r}, \boldsymbol{r}') = \sum_{ij} \phi_i^*(\boldsymbol{r}')\phi_j(\boldsymbol{r})\langle \hat{a}_i^\dagger \hat{a}_j \rangle. \tag{3.21}$$

The density matrix can be diagonalized via an eigenvalue decomposition

$$\rho(\boldsymbol{r}, \boldsymbol{r}') = N \sum_i \lambda_i \tilde{\phi}_i^*(\boldsymbol{r}')\tilde{\phi}_i(\boldsymbol{r}), \tag{3.22}$$

where the $N\lambda_i \geq 0$ are the occupation numbers, normalized such that $\sum_i \lambda_i = 1$, and $\tilde{\phi}_i$ the corresponding orbitals.

Following the criterion of Penrose and Onsager [15], a system is said to undergo Bose-Einstein condensation if one of the eigenvalues, say λ_0, is of the order of unity (i.e., macroscopically occupied). In this case, the system is predominantly condensed in the orbital $\tilde{\phi}_0$.

3.2 Interaction

In one-dimensional systems, a common choice for modeling interactions is the Dirac delta function, $\delta(x)$. However, extending this approach directly to two dimensions introduces significant complications.

When solving the many-body eigenproblem via the variational principle, one typically employs a truncated Fock space and expects that, as the basis size increases, the results converge—that is, they become independent of the cutoff. This convergence generally indicates that the basis adequately captures the systems physics.

Unfortunately, when using the Dirac delta interaction in two dimensions, the calculations exhibit slow divergence as the basis is enlarged. No finite cutoff leads to convergence of the results. This

issue stems from the singular nature of the delta function in higher dimensions, which makes the problem ill-posed unless appropriate regularization is applied (see, e.g., [16, 17]). Alternatively, the interaction strength must be renormalized as a function of the basis size to maintain consistent results [18].

In this thesis, a different approach is adopted: replacing the Dirac delta interaction with a Gaussian potential of the form

$$V(\boldsymbol{r}) = \frac{g}{\sigma^2\pi} e^{r^2/\sigma^2}, \tag{3.23}$$

where g denotes the interaction strength and σ characterizes the width of the potential. The Gaussian provides a smooth, short-range interaction that avoids the singularity and ensures numerical convergence.

To ensure that the Gaussian mimics a contact-like interaction while remaining well-behaved numerically, the width σ is chosen to be smaller that the average interparticle distance. For a system of $N = 6$ particles confined within a disk of radius R, a width of $\sigma = 0.1R$ is used. Estimating the average interparticle distance as $\sqrt{\pi R^2/6} \approx 0.72R$, we find that σ is approximately seven times smaller than this distance confirming that the interaction is sufficiently short-ranged for our purposes.

Now, with the potential determined, we have to calculate the elements V_{ijkl} that appear in the Hamiltonian (3.14). Substituting the Gaussian potential into the general expression (3.15) yields the following double integral (see Appendix A for derivation)

$$V_{ijkl} = \delta^{m_i+m_j}_{m_k+m_l} \iint r r' f_i(r) f_j(r') f_k(r) f_l(r') \frac{4\pi g}{\sigma^2} e^{-\frac{r^2+r'^2}{\sigma^2}} I_{|m_i-m_k|}\left(\frac{2rr'}{\sigma^2}\right) \mathrm{d}r\, \mathrm{d}r', \tag{3.24}$$

where $I_k(x)$ is the modified Bessel function of the first kind, and $f_i(\boldsymbol{r})$ is the radial part of the single-particle orbital ϕ_i.

The Kronecker delta $\delta^{m_i+m_j}_{m_k+m_l}$ enforces conservation of angular momentum in the interaction process. The angular momentum operator,

$$\hat{L}_z = \hbar \sum_i m_i \hat{n}_i, \tag{3.25}$$

commutes with both Hamiltonian $\hat{H}$ and particle number operator $\hat{N}$. Consequently, the eigenvalue problem $\hat{H}|\Psi\rangle = E|\Psi\rangle$ can be solved within a subspace of fixed total particle number and total angular momentum.

3.3 Bogoliubov-de Gennes

In the mean-field approach, a strong simplifying assumption is made: all particles occupy a single-particle orbital $\phi(\boldsymbol{r})$. For stationary systems, this orbital satisfies the equation

$$\left(-\frac{\hbar^2}{2m}\nabla^2 + V_{\mathrm{ex}}(\boldsymbol{r}) + V_{\mathrm{MF}}(\boldsymbol{r})\right)\phi(\boldsymbol{r}) = \mu\phi(\boldsymbol{r}), \tag{3.26}$$

which is known as the Gross-Pitaevskii equation. This framework can be extended using the number conserving Bogoliubov–de Gennes approach, originally developed by Yvan Castin [19, 12]. This extension relaxes the assumption that all particles occupy the mode $\phi(\boldsymbol{r})$, instead positing that the majority do. Within this more refined treatment, the field operator is decomposed as follows:"

$$\hat{\psi}(\boldsymbol{r}) = \phi(\boldsymbol{r})\hat{a}_\phi + \delta\hat{\psi}(\boldsymbol{r}), \tag{3.27}$$

where $\hat{a}_\phi$ annihilates a particle in the orbital $\phi(\boldsymbol{r})$, and $\delta\hat{\psi}(\boldsymbol{r})$ accounts for modes orthogonal to ϕ, satisfying the condition $\int \phi^* \delta\hat{\phi} = 0$. The mean-field approximation is valid when the occupation number operator $\hat{n}_\phi = \hat{a}_\phi^\dagger \hat{a}_\phi$ is of the same order as the total particle number N, such that $1 - N_0/N \ll 1$, where $N_0 = \langle \hat{n}_\phi \rangle$.

The Hamiltonian can then be expanded in powers of $\delta\hat{\psi}$. The zeroth-order term corresponds to the mean-field energy, and it simplifies when $\phi(\boldsymbol{r})$ satisfies the Gross-Pitaevskii equation. The first-order term vanishes due to the same condition. To study the second-order contributions, it is convenient to define a new field operator:

$$\hat{\Lambda}(\boldsymbol{r}) = \frac{1}{\sqrt{\hat{N}}} \hat{a}_0^\dagger \delta\hat{\psi}(\boldsymbol{r}), \tag{3.28}$$

which describes particles transitioning from the non-condensed fraction into the condensed orbital $\phi(\boldsymbol{r})$. Using this operator, the second-order expansion yields a quadratic (Bogoliubov) Hamiltonian:

$$\hat{H}_{\mathrm{q}} = E_{\mathrm{GP}} + \frac{1}{2} \int \mathrm{d}\boldsymbol{r} \begin{pmatrix} \hat{\Lambda}^\dagger & -\hat{\Lambda} \end{pmatrix} \mathcal{L} \begin{pmatrix} \hat{\Lambda} \\ \hat{\Lambda}^\dagger \end{pmatrix}, \tag{3.29}$$

where E_{GP} is the mean-field energy, and $\mathcal{L}$ is the operator:

$$\mathcal{L} = \begin{pmatrix} \hat{H}_{\mathrm{GP}} + \phi\hat{U}^* & \phi\hat{U} \\ -\phi^*\hat{U}^* & -\hat{H}_{\mathrm{GP}} - \phi^*\hat{U} \end{pmatrix}. \tag{3.30}$$

Here, the operator $\hat{H}_{\mathrm{GP}}$ is defined as

$$\hat{H}_{\mathrm{GP}} = -\frac{\hbar^2}{2m}\nabla^2 + V_{\mathrm{MF}}(\boldsymbol{r}) - \mu, \tag{3.31}$$

which depends on the mean-field orbital $\phi(\boldsymbol{r})$ and chemical potential μ. The linear operator $\hat{U}$ describes scattering into and out of the orbital $\phi(\boldsymbol{r})$, and acts on a function $u(\boldsymbol{r})$ via

$$\hat{U}u(\boldsymbol{r}) = (N-1) \int V(|\boldsymbol{r} - \boldsymbol{r}'|)\phi(\boldsymbol{r}')u(\boldsymbol{r}')\,\mathrm{d}\boldsymbol{r}'. \tag{3.32}$$

To use the quadratic Hamiltonian (3.29), one must solve the Bogoliubov-de Gennes eigenvalue problem:

$$\mathcal{L} \begin{pmatrix} u_n \\ v_n \end{pmatrix} = \epsilon_n \begin{pmatrix} u_n \\ v_n \end{pmatrix}, \tag{3.33}$$

with the constraint that $u(\boldsymbol{r})$ and $v(\boldsymbol{r})$ are orthogonal to ϕ and $\phi*$ respectively. This could be simplified by introducing the projection onto the subspace orthogonal to ϕ and ϕ^*, using the projection operators

$$\hat{Q} = 1 - |\phi\rangle\langle\phi|, \tag{3.34}$$

$$\hat{Q}^* = 1 - |\phi^*\rangle\langle\phi^*| \tag{3.35}$$

and replacing $\mathcal{L}$ by

$$\begin{pmatrix} \hat{Q} & 0 \\ 0 & \hat{Q}^* \end{pmatrix} \mathcal{L} \begin{pmatrix} \hat{Q} & 0 \\ 0 & \hat{Q}^* \end{pmatrix}, \tag{3.36}$$

This ensures that $(\,\phi,\,0\,)^{\mathrm{T}}$ and $(\,0,\,\phi^*\,)^{\mathrm{T}}$ become orthogonal eigenvectors, which are typically excluded from further consideration.

The eigenmodes of $\mathcal{L}'$ can be classified into three families based on the value of $\langle u_n|u_n\rangle - \langle v_n|v_n\rangle$:

- 0 family: $\langle u_n|u_n\rangle - \langle v_n|v_n\rangle = 0$
- $+$ family: $\langle u_n|u_n\rangle - \langle v_n|v_n\rangle > 0$
- $-$ family: $\langle u_n|u_n\rangle - \langle v_n|v_n\rangle < 0$

The $+$ and $-$ family modes can be normalized such that $\langle u_n|u_n\rangle - \langle v_n|v_n\rangle = \pm 1$, respectively. The 0-family generally includes only the trivial condesate modes, which are not relevant. Importantly, the sign of the family is unrelated to the sign of the corresponding eigenvalue ϵ_n. However, a negative ϵ_n in the $+$ family indicates thermodynamic instability [12], while a complex ϵ_n signals dynamical instability.

Once the eigenmodes are known, the Bogoliubov-de Gennes approach allows one to compute corrections to the energy:

$$E_{\mathrm{BdG}} = h(N) - \sum_{+\ \text{family}} \epsilon_n \langle v_n|v_n\rangle, \tag{3.37}$$

as well as the depletion of the condensate:

$$\delta N \simeq \sum_{+\ \text{family}} \langle v_n|v_n\rangle. \tag{3.38}$$

Chapter 4

Numerical methods

This chapter is dedicated to the computation methods employed throughout the thesis. We begin be describing the exact diagonalization approach, with particular emphasis on the importance truncation technique. We then present the procedure for sampling particles from the many-body wave function. This is followed by a discussion on solving the mean-field Gross-Pitaevskii equation and the number conserving Bogolibuvo-de Gennes equations. The chapter concludes with technical details regarding the programming language and libraries used in the implementation.

4.1 Exact diagonalization

In the one-dimensional system with Dirac delta-type potential (the Lieb-Liniger model), an analytical solution is available. However, extending the system to two dimensions, necessitates the use of numerical methods. A commonly employed approach in this context is the exact diagonalization of Hamiltonian (3.14).

Any solution to the corresponding eigenvalue problem could be expressed as a linear combination

$$|\Psi\rangle = \sum_{|\boldsymbol{n}\rangle} C_{\boldsymbol{n}} |\boldsymbol{n}\rangle, \tag{4.1}$$

where the coefficients $C_{\boldsymbol{n}}$ are normalized to unity $\sum |C_{\boldsymbol{n}}|^2 = 1$. Given that the full Fock space is infinite-dimensional, numerical implementation requires a truncation scheme.

We define $\mathcal{B}$ as a finite computational basis of Fock states, typically constrained by physical quantities. A basis state $|\boldsymbol{n}\rangle \in \mathcal{B}$ satisfies $\sum n_i = N$ and $\sum m_i n_i = M$ where N is the total particle number and M is the total angular momentum in units of $\hbar$. Thus, the numerical calculation is performed in a finite-dimensional subspace $\mathcal{F} = \operatorname{span} \mathcal{B}$ characterized by fixed total particle number and angular momentum.

Diagonalizing the Hamiltonian within this subspace yields an approximation to the true eigenstates of the full system.

A natural question arises: how do we decide what Fock states be selected for inclusion in the computational basis $\mathcal{B}$? The straightforward truncation strategies are commonly considered:

- *Single-particle cutoff*: A basis state $|\boldsymbol{n}\rangle \in \mathcal{B}$ is included only if $n_i = 0$ for $i > i_{\text{cut}}$. Here $i_{\text{cut}} \in \mathbb{N}$ serves as a cutoff parameter for the single-particle states indices.
- *Many-body energy cutoff*: A basis state $|\boldsymbol{n}\rangle \in \mathcal{B}$ is included if the total non-interacting energy $\sum E_i n_i$ is less than some threshold E_{cut}, where E_i are the single-particle energy levels. In this case, E_{cut} is the tunable cutoff parameter.

While both approaches are conceptually simple, they suffer from a rapid growth in the size of the basis with increasing i_{cut} or E_{cut}, which means, in practice, that computations are limited to parameter regimes with weak interactions only.

Moreover, these methods are agnostic to the specific features of the interacting Hamiltonian. As a result, they tend to include many basis states that contribute little to the actual physical

solution. A more refined strategy, known as *importance truncation* [11], addresses this issue by selecting basis states based on their estimated relevance to the specific many-body Hamiltonian.

The importance truncation method relies on the iterative construction of the computational basis $\mathcal{B}$. Suppose we are interested in approximating the ground state of the system. The procedure begins by defining an initial, small basis $\mathcal{B}_1$ which may consist of just a few Fock states — or even a single one. Solving the eigenvalue problem

$$\hat{H}|\Psi^1_{\text{ref}}\rangle = E^1_{\text{ref}}|\Psi^1_{\text{ref}}\rangle \tag{4.2}$$

within this subspace yields a first approximation to the ground state, referred to as the *reference state*, which takes the form

$$|\Psi^1_{\text{ref}}\rangle = \sum_{|\boldsymbol{n}\rangle\in\mathcal{B}_1} C^1_{\boldsymbol{n}}|\boldsymbol{n}\rangle. \tag{4.3}$$

Next, we define a larger set $\mathcal{B}_{\text{s}}$ —the *search space*—constructed using one of the more naive truncation schemes discussed earlier (such as energy or single-particle cutoffs). This set serves as a reservoir of candidate basis states. The goal is to identify states in $\mathcal{B}_{\text{s}}$ that are potentially important for improving the reference solution.

To do so, we assign an *importance measure* to each candidate state $|\boldsymbol{n}\rangle \in \mathcal{B}_{\text{s}} \setminus \mathcal{B}_1$ based on first-order perturbation theory:

$$\kappa_{\boldsymbol{n}} = \left| \frac{\langle \Psi^1_{\text{ref}}|V|\boldsymbol{n}\rangle}{E_{\boldsymbol{n}} - E_0} \right|, \tag{4.4}$$

where $E_{\boldsymbol{n}}$ is the noninteracting Fock energy ($\hat{H}|\boldsymbol{n}\rangle = E_{\boldsymbol{n}}|\boldsymbol{n}\rangle$ when $\hat{V} = 0$), with E_0 corresponding to the ground state. A new, enlarged basis $\mathcal{B}_2$ is then constructed by combining $\mathcal{B}_1$ with those states from $\mathcal{B}_{\text{s}}$ that satisfy the importance criterion:

$$\mathcal{B}_2 = \mathcal{B}_1 \cup \{\, |\boldsymbol{n}\rangle \in \mathcal{B}_{\text{s}} \setminus \mathcal{B}_1 \mid \kappa_{\boldsymbol{n}} \geq \kappa_{\min} \,\}. \tag{4.5}$$

The process is then repeated iteratively, constructing successive bases $\mathcal{B}_3, \mathcal{B}_4, \ldots$ until convergence is achieved—typically determined by checking that the computed ground-state energy E_{ref} stabilizes between iterations.

In practice, an additional parameter $C_{\min}$ can be introduced to refine the calculation of $\kappa_{\boldsymbol{n}}$. Instead of using the full reference state $|\Psi^1_{\text{ref}}\rangle$, one can define a truncated version $|\Psi^1_{\text{ref}}\rangle'$, constructed by retaining only coefficients $|C^1_{\boldsymbol{n}}| \geq C_{\min}$, followed by renormalization:

$$|\Psi^1_{\text{ref}}\rangle' = \frac{1}{\sqrt{\mathcal{N}}} \sum_{|C^1_{\boldsymbol{n}}|\geq C_{\min}} C_{\boldsymbol{n}}|\boldsymbol{n}\rangle, \;\text{ with }\; \mathcal{N} = \sum_{|C^1_{\boldsymbol{n}}|\geq C_{\min}} |C^1_{\boldsymbol{n}}|^2. \tag{4.6}$$

To verify convergence and assess accuracy, one must examine the sensitivity of the resulting energies to the parameters $\kappa_{\min}$, $C_{\min}$, and the choice of search space $\mathcal{B}_{\text{s}}$. In our calculations, the values $\kappa_{\min} = 10^{-5}$ and $C_{\min} = 10^{-4}$ were found to provide reliable and stable results.

When constructing the search set $\mathcal{B}_{\text{s}}$, it was found that applying an energy cutoff on the many-body states is generally more effective than using a cutoff on the single-particle orbitals. The key

E_{cut}	size of $\mathcal{B}_{\text{s}}$
200	36'943
400	1'921'885
600	19'481'375
800	100'500'179
1000	357'937'806
1200	1'008'552'286

Table 4.1: Size of the importance truncation search space $\mathcal{B}_{\text{s}}$ for increasing values of the energy cutoff E_{cut}.

reason lies in the fact that some crucial many-body configurations may involve only one or two high-energy single-particle states. Such configurations can be completely missed when relying solely on a single-particle cutoff, as the necessary orbitals may not yet be included.

Another drawback of single-particle cutoff schemes is the difficulty of reaching important orbitals due to angular momentum constrains. For instance, a single-particle state ϕ_i with index $i = 539$ carries angular momentum $25\hbar$, which is quite large. In order to construct a total many-body state with zero angular momentum, such a component would require another state with nearly equal and opposite angular momentum (or few states with smaller angular momentum). In contrast, a state like ϕ_{516}, which has zero angular momentum, can be included without changing the total angular momentum and is thus more likely to contribute significantly to the low-energy spectrum.

Table 4.1 illustrates how the size of the search space $\mathcal{B}_{\text{s}}$ grows with increasing energy cutoff E_{cut}, under the constraint of total angular momentum $0\hbar$ and number of particles $N = 6$. This exponential growth underscores the need for effective truncation strategies such as importance truncation. Meanwhile, Fig. 4.1 shows how the computed ground-state energy varies with respect to E_{cut}, demonstrating convergence behavior.

When computing the importance measure $\kappa_{\min}$, we must evaluate the matrix elements

$$\langle \Psi^1_{\text{ref}} | V | \boldsymbol{n} \rangle = \sum_{\boldsymbol{n}'} C^{1*}_{\boldsymbol{n}'} \langle \boldsymbol{n}' | V | \boldsymbol{n} \rangle. \tag{4.7}$$

To make this computation efficient, we can exploit the structure of the interaction operator $\hat{V}$, which consists of a products of two creation and two annihilation operators $\hat{a}^\dagger_i \hat{a}^\dagger_j \hat{a}_l \hat{a}_k$. As a consequence, the matrix element $\langle \boldsymbol{n}' | V | \boldsymbol{n} \rangle$ is nonzero only if the state $|\boldsymbol{n}\rangle$ can be obtained from $|\boldsymbol{n}'\rangle$ by moving at most two particles between orbitals.

This observation allows us to significantly reduce the number of matrix elements we need to compute. Instead of looping over the entire search space $\mathcal{B}_{\text{s}}$, we can iterate over the states $|\boldsymbol{n}'\rangle$ with nonzero amplitudes $C^1_{\boldsymbol{n}'}$ in the reference state $|\Psi^1_{\text{ref}}\rangle$, and then generate all states $|\boldsymbol{n}\rangle$ that are reachable from each $|\boldsymbol{n}'\rangle$ via two-body transitions. During this process, we can also track the excitation energy of the candidate state $|\boldsymbol{n}\rangle$ to check whether it falls within the energy cutoff defining $\mathcal{B}_{\text{s}}$.

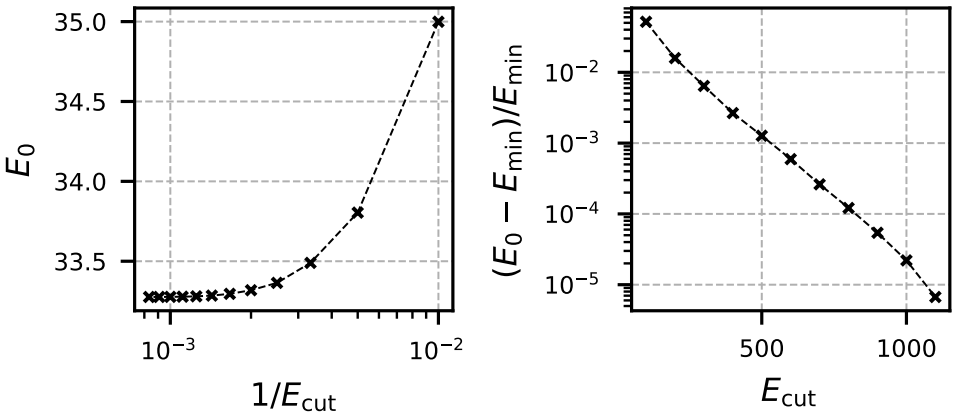

Figure 4.1: Convergence of the ground state energy using exact diagonalization with the importance truncation scheme. The left panel shows the ground state energy as function of the inverse energy cutoff $1/E_{\text{cut}}$ used to define the truncation search space $\mathcal{B}_{\text{s}}$. The right panel displays the relative error of the ground state energy with respect to the lowest value, plotted as a function of E_{cut}. The results are shown for a system of $N = 6$ particles at the hightest considered interaction strength, $gN = 18\ \hbar^2/m$. The importance truncation parameters used are $\kappa_{\text{min}} = 10^{-5}$ and $C_{\text{min}} = 10^{-4}$.

In order to evaluate matrix elements $\langle \boldsymbol{n}'|V|\boldsymbol{n}\rangle$, we require the two-body integrals V_{ijkl} defined by (3.15). These integrals can be computed on demand and stored in memory for reuse through the calculation. Furthermore, they may be written to disk at the end of a computation to be loaded in subsequent runs, thus avoiding unnecessary recomputation and improving overall efficiency.

A crucial step in the importance truncation scheme—and in solving the many-body problem in general—is the diagonalization of the Hamiltonian matrix. Since we are typically interested only in the ground state, full diagonalization becomes computationally inefficient for large matrices. Instead, the Lanczos algorithm offers a much more practical alternative. It is particularly well-suited for large, sparse matrices—an advantage that applies here, as more that 99% of the Hamiltonian matrix elements in our system are zero.

Using the Lanczos method, we were able to efficiently diagonalize Hamiltonians with dimensions up to 300'000, enabling accurate ground-state approximations within a reasonable computational time frame.

4.2 Particles drawing

To investigate the *conditional wave function* $\psi_{\text{cond}}(\bar{\boldsymbol{r}}_1, \ldots, \bar{\boldsymbol{r}}_{N-1}, \boldsymbol{r})$ we need to sample (i.e., measure) the position of $N-1$ particles. In principle, this requires drawing samples from a probability distribution defined over a $D \times N$-dimensional space, where D is the spatial dimension of the system (for example, D=2 for our system).

Instead of sampling all coordinates simultaneously, we adopt a sequential sampling approach, drawing particle positions one at a time. The method begins by sampling the position of the

second particle, $\bar{\boldsymbol{r}}_1$, from a distribution proportional to the single-particle density:

$$\rho_1(\boldsymbol{r}) \propto \int |\Psi(\boldsymbol{r}_1, \boldsymbol{r}_2, \ldots, \boldsymbol{r}_{N-1}, \boldsymbol{r})|^2 \, \mathrm{d}\boldsymbol{r}_1 \cdots \mathrm{d}\boldsymbol{r}_{N-1}. \tag{4.8}$$

Once $\bar{\boldsymbol{r}}_1$ has been obtained, the next position $\bar{\boldsymbol{r}}_2$ is drawn from

$$\rho_2(\boldsymbol{r}) \propto \int |\Psi(\bar{\boldsymbol{r}}_1, \boldsymbol{r}_2, \ldots, \boldsymbol{r}_{N-1}, \boldsymbol{r})|^2 \, \mathrm{d}\boldsymbol{r}_2 \cdots \mathrm{d}\boldsymbol{r}_{N-1}, \tag{4.9}$$

and this process continues iteratively until all $N-1$ positions have been fixed.

However, evaluating such high-dimensional integrals of a many-body wave function is computationally expensive and generally impractical. A more suitable approach within the Fock space formalism is to implement this sampling procedure with the aid of second quantization.

Let us denote the initial many-body wave function by $|\Psi_1\rangle$. The first particle position $\bar{\boldsymbol{r}}_1$ is drawn from the probability density

$$\rho_1(\boldsymbol{r}) \propto \langle \Psi_1 | \hat{\psi}^\dagger(\boldsymbol{r}) \hat{\psi}(\boldsymbol{r}) | \Psi_1 \rangle. \tag{4.10}$$

Once the position $\bar{\boldsymbol{r}}_1$ is sampled, we construct a new $(N-1)$-particle state by acting with the field annihilation operator:

$$|\Psi_2\rangle = \hat{\psi}(\bar{\boldsymbol{r}}_1) |\Psi_1\rangle. \tag{4.11}$$

This new state $|\Psi_2\rangle$ depends explicitly on the previously sampled coordinate. The next particle position $\bar{\boldsymbol{r}}_2$ is drawn from the corresponding density:

$$\rho_2(\boldsymbol{r}) \propto \langle \Psi_2 | \hat{\psi}^\dagger(\boldsymbol{r}) \hat{\psi}(\boldsymbol{r}) | \Psi_2 \rangle \tag{4.12}$$

and the procedure is repeated recursively. In general, the n-th position is drawn from

$$\rho_n(\boldsymbol{r}) \propto \langle \Psi_n | \hat{\psi}^\dagger(\boldsymbol{r}) \hat{\psi}(\boldsymbol{r}) | \Psi_n \rangle \tag{4.13}$$

with the n-particle wave function defined recursively as:

$$|\Psi_n\rangle = \hat{\psi}(\bar{\boldsymbol{r}}_{n-1}) |\Psi_{n-1}\rangle. \tag{4.14}$$

This yields a sequence of $N-1$ sampled positions $\bar{\boldsymbol{r}}_1, \ldots, \bar{\boldsymbol{r}}_{N-1}$, which can then be used to construct and analyze the conditional wave function ψ_{cond}.

4.3 Mean field and Bogoliubov-de Gennes

Our goal is to solve the mean-field equation of the form:

$$\left(-\frac{\hbar^2}{2m} \nabla^2 + V_{\mathrm{ex}}(\boldsymbol{r}) + V_{\mathrm{MF}}(\boldsymbol{r}) \right) \phi(\boldsymbol{r}) = \mu \phi(\boldsymbol{r}), \tag{4.15}$$

with a focus on two particular solutions. The first is the ground state, which is assumed to be radially symmetric $\phi_0 = f_0(r)$. The second is a state carrying a single vortex at the origin, taking the form $\phi_1(\boldsymbol{r}) = f_1(r) e^{i\theta}$.

To solve the Gross-Pitaevskii equation, we employ a self-consistent approach using a single-particle basis expansion. Specifically, we search for solutions of the form

$$\phi_m(\boldsymbol{r}) = \sum_{i,\ m_i=m} c_i \psi_i(\boldsymbol{r}) \tag{4.16}$$

where m denotes the total angular momentum in $\hbar$ (0 or 1) and in the sum we take into account only those orbitals that have the angular momentum m, so $m_i = m$. The coefficients are normalized, $\sum |c_i|^2 = 1$.

Starting from an initial normalized guess defined by the coefficients c_i, we construct the matrix representation of the mean-field operator

$$-\frac{\hbar^2}{2m}\nabla^2 + V_{\text{ex}}(\boldsymbol{r}) + V_{\text{MF}}(\boldsymbol{r}) \tag{4.17}$$

where the mean-field potential V_{MF} is computed based on the current approximation of the solution. Diagonalizing this operator yields a new set of eigenstates, and the state corresponding to the lowest eigenvalue is used as the updated guess.

This iterative procedure continues until the chemical potential μ converges within a specified tolerance. To improve convergence, we found it effective to apply a mixing strategy: instead of replacing the old solution entirely, we update it using a weighted combination of the old and new states. Empirically, using a mixture of 0.2 (old) and 0.8 (new) proved to work well.

Once the GPE solution $\phi_m(\boldsymbol{r})$ has been obtained, we proceed to solve the Bogoliubov-de Gennes (BdG) equations:

$$\mathcal{L}' \begin{pmatrix} u_n \\ v_n \end{pmatrix} = \epsilon_n \begin{pmatrix} u_n \\ v_n \end{pmatrix}, \tag{4.18}$$

where the transformed BdG operator $\mathcal{L}'$ is defined by

$$\mathcal{L}' = \begin{pmatrix} \hat{Q} & 0 \\ 0 & \hat{Q}^* \end{pmatrix} \mathcal{L} \begin{pmatrix} \hat{Q} & 0 \\ 0 & \hat{Q}^* \end{pmatrix}, \tag{4.19}$$

with $\hat{Q} = 1 - |\phi_m\rangle\langle\phi_m|$, $\hat{Q}^* = 1 - |\phi_m^*\rangle\langle\phi_m^*|$, and the original BdG operator $\mathcal{L}$ takes the form

$$\mathcal{L} = \begin{pmatrix} \hat{H}_{\text{GP}} + \phi_m \hat{U}^* & \phi_m \hat{U} \\ -\phi_m^* \hat{U}^* & -\hat{H}_{\text{GP}} - \phi_m^* \hat{U} \end{pmatrix}. \tag{4.20}$$

Since the BdG equations are linear, the problem reduces to a matrix diagonalization in an appropriate basis. We construct this basis from the single-particle orbitals ψ_i, representing states as either $(\,\psi_i,\, 0\,)^T$ or $(\,0,\, \psi_i\,)^T$.

The matrix structure imposes angular momentum selection rules:

- $(\,\psi_i,\, 0\,)^T$ couples to $(\,\psi_j,\, 0\,)^T$ only when $m_i = m_j$.
- $(\,0,\, \psi_i\,)^T$ couples to $(\,0,\, \psi_j\,)^T$ only when $m_i = m_j$.
- $(\,\psi_i,\, 0\,)^T$ couples to $(\,0,\, \psi_j\,)^T$ only if the condition of the form $m_i = 2m + m_j$ is satisfied.

These angular momentum constraints effectively partition the Hilbert space into independent subspaces, allowing us to solve (4.18) in blocks corresponding to conserved angular momentum sectors. Physically, these selection rules reflect angular momentum conservation in the system.

4.4 Technical details

The numerical methods described in this thesis have been implemented in C++ with the aid of the following libraries:

- *GSL - GNU Scientific library* [20] - used for computing Bessel functions and their zeros;
- *Eigen* [21] - for basic linear algebra operations;
- *Spectra* [22] – used for its implementation of the Lanczos algorithm for sparse matrix diagonalization. This library depends on *Eigen*.

Most of the figures and data visualizations were generated using Python, employing the *numpy*, *scipy*, and *matplotlib* libraries. The data, along with Python scripts used to generate a large portion of the figures, is freely available at [23].

The code used for solving the many-body problem using importance trunction, solving the GPE and BdG equation is available at [24].

Chapter 5

Results

5.1 Quntities

We begin our investigation of the system by examining the energy as a function of interaction strength, as shown in Fig. 5.1. This comparison allows us to assess the consistency between the many-body (MB) and mean-field (MF) approaches. The calculations were carried out for a system of $N = 6$ particles, and we have plotted the two lowest-energy states at fixed angular momentum—referred to as yrast states. The many-body energies are represented by solid lines: yellow for the yrast state with $L_z = 0$, and blue for $L_z = N\hbar$. The energy obtained from the Gross-Pitaevskii equation is shown with black dashed line, while the Bogoliubov-de Gennes corrections to the mean-field results are depicted using red dot-dashed lines.

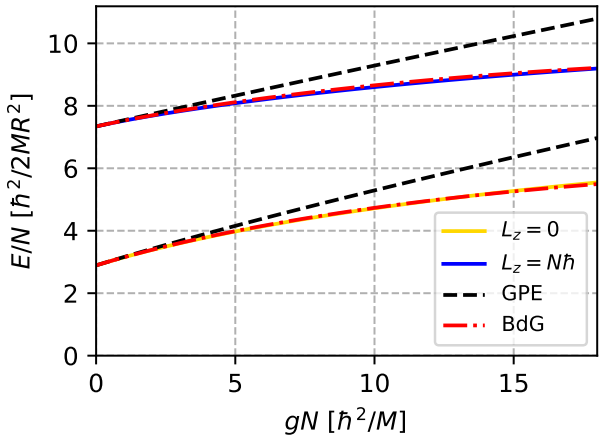

Figure 5.1: Energy as a function of interaction strength for the yrast states with $L_z = 0$ (yellow solid line) and $L_z = N\hbar$ (blue solid line), compared with the mean-field energy (black dashed line) and the Bogoliubov–de Gennes correction (red dot-dashed line). The calculations were performed for $N = 6$ particles with a Gaussian width of $\sigma = 0.1R$.

We observe that the mean-field results closely follow the many-body energies only at low interaction strengths, with both approaches exhibiting the same derivative at $g = 0$. In contrast, the Bogoliubov–de Gennes (BdG) correction closely matches the many-body results across the entire range of interaction strengths considered.

Another important figure of merit is the condensate fraction, which provides insight into the degree of condensate depletion and indicates the range of interaction strengths where the Gross-Pitaevskii (GP) description remains valid. We compute the condensate fraction for both $L_z = 0$ and $L_z = N\hbar$ across the same range of interaction strengths, as shown in Fig. 5.2. The yellow curve, corresponding to $L_z = 0$, shows that the system remains mostly condensed. In contrast, the $L_z = N\hbar$ case exhibits significantly higher depletion, indicating that the vortex state tends to lose more particles from the condensate compared to the non-rotating ground state.

We also calculate the condensate fraction using the BdG correction to the GP description, shown as the red dot-dashed line. While it generally follows the many-body result, it noticeable deviates, especially for $L_z = N\hbar$

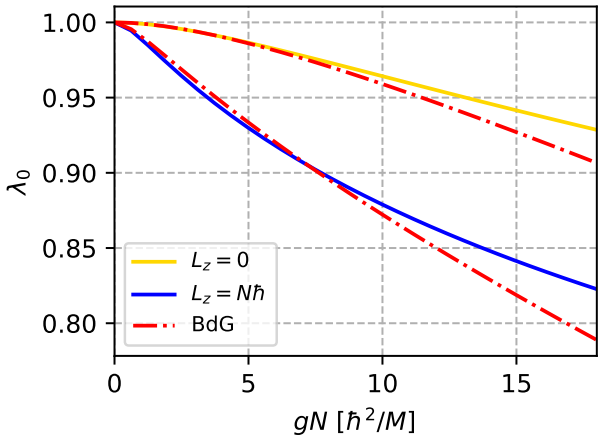

Figure 5.2: Condensate fraction as a function of interaction strength for the yrast states with $L_z = 0$ (yellow solid line) and $L_z = N\hbar$ (blue solid line), along with the corresponding Bogoliubov–de Gennes prediction (red dot-dashed line). Calculations were performed for $N = 6$ particles with a Gaussian width $\sigma = 0.1R$.

Next, we examine the particle densities. In the mean-field approximation, the density is simply given by $N|\phi|^2$, where ϕ denotes the macroscopically occupied orbital. From the many-body solution, we compute the diagonal of the single-particle density matrix, which provides the average particle density.

For the case of $L_z = 0$ and several values of the interaction strength, cross-sections of the densities along the center of the system are shown in Fig. 5.3. The solid yellow lines represent the densities obtained from the many-body calculation, while the black dashed lines correspond to the mean-field results. We observe that the mean-field density closely matches the many-body density across the entire interaction range considered. This agreement is consistent with the low level of condensate depletion previously observed.

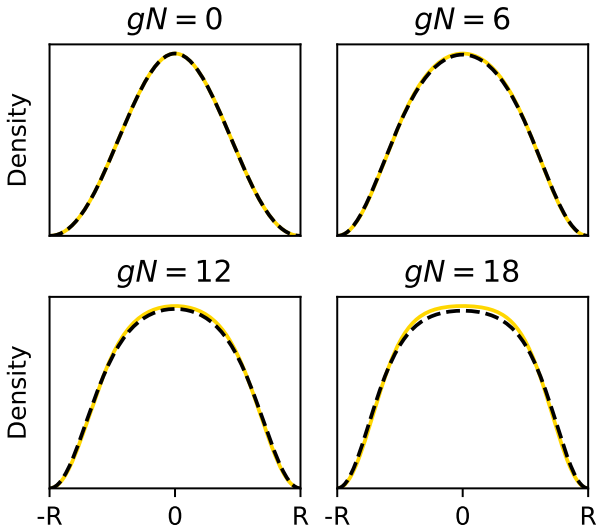

Figure 5.3: Density profiles for several interaction strengths for the $L_z = 0$ yrast state, obtained from the single-particle density matrix (yellow solid lines) and the mean-field approximation (black dashed lines). Calculations were carried out for $N = 6$ particles with a Gaussian width $\sigma = 0.1R$.

We now turn to the case of $L_z = N\hbar$, where we expect greater discrepancies between the mean-field and many-body descriptions, as suggested by the condensate fraction shown in Fig. 5.2. Indeed, Fig. 5.4 illustrates that as the interaction strength increases, the many-body density (blue solid line) increases at the center of the disk. In contrast, the mean-field density (black dashed line) consistently drops to zero at the center, reflecting the presence of a well-defined vortex core.

The orbitals into which particles are depleted from the vortex state can be identified using the Bogoliubov–de Gennes (BdG) approach. These are shown in Fig. 5.5, where we plot the two most significantly occupied Bogoliubov modes. They indicate that particles predominantly transition from the vortex state to orbitals with angular momenta $L_z = 0$ and $L_z = 2\hbar$, in equal proportions—thus preserving the total angular momentum of the system.

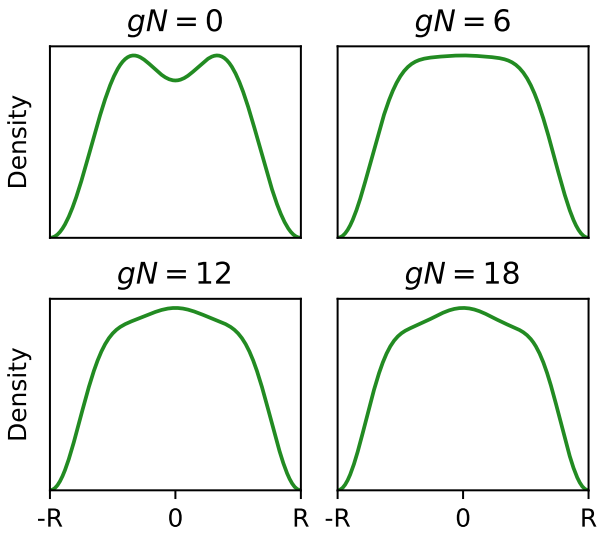

Figure 5.4: Density profiles for several interaction strengths for the $L_z = N\hbar$ yrast state, shown using the single-particle density matrix (blue solid lines) and the mean-field approximation (black dashed lines). The calculations were performed for $N = 6$ particles with a Gaussian width $\sigma = 0.1R$.

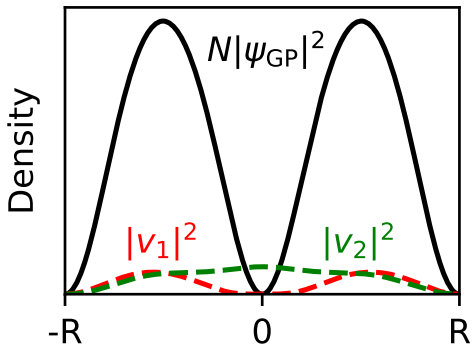

Figure 5.5: Density of the mean-field orbital (black dashed line) shown alongside the densities $|v|^2$ of the two most highly occupied Bogoliubov–de Gennes modes. These two modes have approximately equal occupation and angular momenta $L_z = 0$ and $L_z = 2\hbar$, ensuring that the total angular momentum per particle remains at $N\hbar$. Calculations were performed for $N = 6$ particles, interaction strength $gN = 18\hbar^2/m$, and Gaussian width $\sigma = 0.1R$.

Even though the density is nonzero at the center, the presence of a vortex remains clearly visible in the case of $L_z = N\hbar$. We now turn to a more subtle scenario, where the total angular momentum lies between 0 and $N\hbar$. Intuitively, one might expect the vortex to be located off-center in such cases. However, as shown in Fig. 5.6, the single-particle density matrix for $L_z = \frac{N}{2}\hbar$ does not reveal a clearly defined vortex core—the averaged density obscures its presence.

Moreover, comparison with the stationary Gross-Pitaevskii solution becomes nontrivial. A vortex displaced from the center would naturally rotate around it, making a time-independent (stationary) solution inappropriate. As a result, no corresponding mean-field line is shown in the figure.

To resolve the vortex structure in such intermediate angular momentum states, we must turn to alternative methods. Specifically, we employ the position-measurement-based approach described in Section (XXX), which allows us to extract more detailed spatial information beyond what is visible in the averaged density profile.

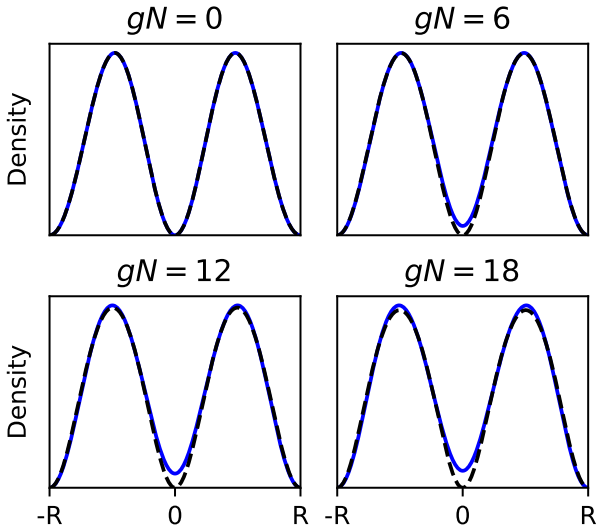

Figure 5.6: Density profiles for several interaction strengths for the $L_z = \frac{N}{2}\hbar$ yrast state, obtained from the single-particle density matrix (green solid lines) and the mean-field approximation (black dashed lines). Calculations were performed for $N = 6$ particles with a Gaussian width $\sigma = 0.1R$.

5.2 Vortex in the many body wave function

To identify the vortex structures in the N-body wave function, we employ the method described in Section **XXX**. In this approach, we fix the positions of $N-1$ particles, denoted by $\bar{\boldsymbol{r}}_1, \ldots, \bar{\boldsymbol{r}}_{N-1}$, and examine the resulting conditional wave function of the remaining particle:

$$\psi_{\text{cond}}(\boldsymbol{r}) = \Psi(\boldsymbol{r}, \bar{\boldsymbol{r}}_1, \ldots, \bar{\boldsymbol{r}}_{N-1}). \tag{5.1}$$

This function provides insight into the phase and density structure of the full many-body wave function, conditioned by specific measured positions $\bar{\boldsymbol{r}}_1, \ldots, \bar{\boldsymbol{r}}_{N-1}$.

We carry out the position-sampling procedure for a system of $N = 6$ particles at an interaction strength of $gN = 18\hbar^2/m$. This yields multiple sets of particle positions, from which we construct the corresponding conditional wave functions. Examples are shown in Fig. 5.7, where each configuration is decomposed into its density and phase components. Panel (a) presents five examples for $L_z = \frac{N}{2}\hbar$, while panel (b) shows five examples for $L_z = N\hbar$.

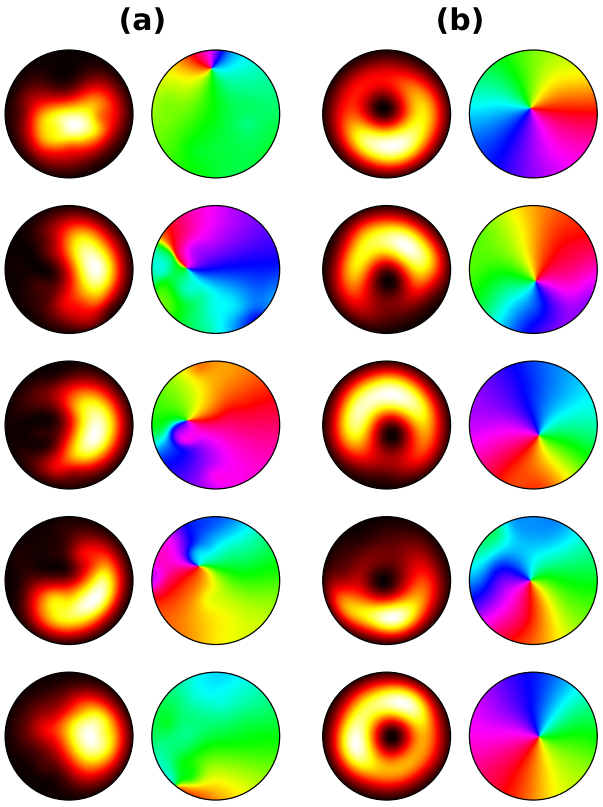

Figure 5.7: Conditional wave functions for $L_z = \frac{N}{2}\hbar$ (panel a) and $L_z = N\hbar$ (panel b). In each panel, the left column shows the density and the right column shows the phase of ψ_{cond}. When present, vortices appear off-center; this positional variation is more pronounced in panel (a). Calculations were performed for $N = 6$ particles, interaction strength $gN = 18\hbar^2/m$, and Gaussian width $\sigma = 0.1R$.

In most realizations of the sampling procedure, a vortex is clearly observed; however, its position varies between different sets of measured particle positions. The vortices obtained in this manner are dynamically stable in the sense that, when the conditional wave function is used as the initial state in the time-dependent Gross–Pitaevskii equation, it evolves in a stable manner. For weaker interactions ($gN = 6\hbar^2/m$), the vortex core rotates smoothly around the center of the disk with minimal disturbance. For stronger interactions ($gN = \frac{N}{2}\hbar$), the evolution becomes more perturbed. An animation of this time evolution is provided as supplementary material in [25].

If one averages the density profiles obtained from many conditional wave function realizations, the result converges to the single-particle density matrix. As we have already observed, this averaged density does not reveal the presence of a vortex, due to the large spread in vortex positions across different realizations.

The case of $L_z = N\hbar$, shown in panel (b) of Fig. 5.7, is somewhat different. The vortex images closely resemble the mean-field vortex structure, but with a slight offset from the center. This is consistent with the nonzero central density observed in the single-particle density matrix. The spread in vortex positions in this case is likely related to the Bogoliubov–de Gennes modes discussed earlier.

Chapter 6

Conclusions

In this master thesis, we investigate the emergence of a quantum vortex—an object best understood within the framework of the mean-field approximation—as it appears in the solution to the many-body Schrödinger equation describing interacting bosons.

Before focusing on vortices, in Chapter 2, we reviewed the foundational concepts of many-body quantum mechanics, beginning with the structure of the N-body wave function and the symmetry constraints imposed by indistinguishability of bosons. We introduced the single-particle density matrix and derived the Gross-Pitaevskii equation (GPE) for systems with non-local interactions. We then explored how solitons arise in the one-dimensional Lieb-Liniger model, particularly through the analysis of conditional wave functions following simulated position measurements. This chapter concluded with the introduction of quantum vortices as macroscopic excitations described by the mean-field orbital obtained from the GPE.

In Chapter 3, we presented our model: a two-dimensional disk confining interacting bosons. We reformulated the problem using second quantization and introduced the Penrose-Onsager criterion for Bose-Einstein condensation, based on the eigenstructure of the single-particle density matrix. A Gaussian-like repulsive interaction potential was defined, and we emphasized that this choice conserves the total angular momentum of the system. We also briefly introduced the number-conserving Bogoliubov–de Gennes (BdG) formalism, providing the expressions for the energy corrections and condensate depletion.

Chapter 4 focused on the numerical methods used. We described the exact diagonalization technique, how we constructed and truncated the computational basis, and how this process was improved via importance truncation. To ensure the reliability of our results, we presented convergence plots of the ground state energy as a function of the cutoff energy. A key component of this work—the iterative "measurement" procedure used to extract particle positions one by one from the many-body wave function—was described in detail. We also outlined the numerical methods used to solve the GPE and BdG equations, and concluded the chapter with implementation details such as the programming language, libraries, and the source code.

In Chapter 5, we presented the main results of our simulations. We compared energies and condensate depletion between the mean-field and many-body descriptions, and analyzed density cross-sections at different total angular momenta. We visualized the BdG modes associated with the single-vortex state, showing how particles are excited out of the condensate. Most importantly, we demonstrated the emergence of vortices through conditional wave function measurements, revealing random vortex positions in each trial. We observed that vortices typically appear off-center and linked this spatial spread to the structure of the BdG modes.

This work opens several avenues for further research. Preliminary investigations (not presented here) suggest that vortex lattices can emerge at angular momenta exceeding $N\hbar$, though these results require proper convergence checks and more systematic study. The dynamics of vortices under the time-dependent Schrödinger equation remain largely unexplored and would be a natural extension. Moreover, thermal effects are entirely absent from this analysis. Including

temperature effects—particularly in two-dimensional systems—would allow one to explore phenomena such as the Berezinskii-Kosterlitz-Thouless (BKT) transition. Investigating such effects might be feasible using alternative geometries, such as periodic boundary conditions.

Finally, since we have demonstrated that the measurement-based approach successfully reveals vortex structures—just as it did for solitons in one-dimensional systems—there is strong motivation to apply this technique to study other emergent quantum structures, such as quantum droplets, in future work.

Bibliography

[1] Elliott H. Lieb and Werner Liniger. Exact analysis of an interacting bose gas. i. the general solution and the ground state. *Phys. Rev.*, 130:1605–1616, May 1963.

[2] Elliott H. Lieb. Exact analysis of an interacting bose gas. ii. the excitation spectrum. *Phys. Rev.*, 130:1616–1624, May 1963.

[3] Masakatsu Ishikawa and Hajime Takayama. Solitons in a one-dimensional bose system with the repulsive delta-function interaction. *Journal of the Physical Society of Japan*, 49(4):1242–1246, 1980.

[4] Andrzej Syrwid and Krzysztof Sacha. Lieb-liniger model: Emergence of dark solitons in the course of measurements of particle positions. *Physical Review A*, 92(3):032110, 2015.

[5] Andrzej Syrwid, Mirosław Brewczyk, Mariusz Gajda, and Krzysztof Sacha. Single-shot simulations of dynamics of quantum dark solitons. *Physical Review A*, 94(2):023623, 2016.

[6] J. R. Abo-Shaeer, C. Raman, J. M. Vogels, and W. Ketterle. Observation of vortex lattices in bose-einstein condensates. *Science*, 292(5516):476–479, 2001.

[7] V. L. Berezinsky. Destruction of long range order in one-dimensional and two-dimensional systems having a continuous symmetry group. I. Classical systems. *Sov. Phys. JETP*, 32:493–500, 1971.

[8] J. M. Kosterlitz and D. J. Thouless. Ordering, metastability and phase transitions in two-dimensional systems. *J. Phys. C: Solid State Phys.*, 6(7):1181, Apr 1973.

[9] Zoran Hadzibabic, Peter Krüger, Marc Cheneau, Baptiste Battelier, and Jean Dalibard. Berezinskii–Kosterlitz–Thouless crossover in a trapped atomic gas. *Nature*, 441:1118–1121, June 2006.

[10] E. A. L. Henn, J. A. Seman, G. Roati, K. M. F. Magalhães, and V. S. Bagnato. Emergence of turbulence in an oscillating bose-einstein condensate. *Phys. Rev. Lett.*, 103:045301, Jul 2009.

[11] Robert Roth. Importance truncation for large-scale configuration interaction approaches. *Phys. Rev. C*, 79:064324, Jun 2009.

[12] Y. Castin. Bose-Einstein Condensates in Atomic Gases: Simple Theoretical Results. In *Coherent atomic matter waves*, pages 1–136. Springer, Berlin, Germany, Jul 2002.

[13] Andrzej Syrwid and Krzysztof Sacha. Lieb-liniger model: Emergence of dark solitons in the course of measurements of particle positions. *Phys. Rev. A*, 92:032110, Sep 2015.

[14] R. Ołdziejewski, W. Górecki, K. Pawłowski, and K. Rzążewski. Many-body solitonlike states of the bosonic ideal gas. *Phys. Rev. A*, 97:063617, Jun 2018.

[15] Oliver Penrose and Lars Onsager. Bose-einstein condensation and liquid helium. *Phys. Rev.*, 104:576–584, Nov 1956.

[16] Lawrence R. Mead and John Godines. An analytical example of renormalization in two-dimensional quantum mechanics. *Am. J. Phys.*, 59(10):935–937, October 1991.

[17] Christophe Mora and Yvan Castin. Extension of bogoliubov theory to quasicondensates. *Phys. Rev. A*, 67:053615, May 2003.

[18] Massimo Rontani, G Eriksson, S Åberg, and S M Reimann. On the renormalization of contact interactions for the configuration-interaction method in two-dimensions. *Journal of Physics B: Atomic, Molecular and Optical Physics*, 50(6):065301, mar 2017.

[19] Y. Castin and R. Dum. Low-temperature bose-einstein condensates in time-dependent traps: Beyond the $u(1)$ symmetry-breaking approach. *Phys. Rev. A*, 57:3008–3021, Apr 1998.

[20] Gsl - gnu scientific library. Access: 13.05.2025 r., http://www.gnu.org/software/gsl/.

[21] Gaël Guennebaud, Benoît Jacob, et al. Eigen v3. http://eigen.tuxfamily.org, 2010.

[22] Spectra - sparse eigenvalue computation toolkit as a redesigned arpack. Access: 13.05.2025 r., https://spectralib.org/.

[23] Mateusz Ślusarczyk. Dataset for "vortices in the many-body excited states of interacting bosons in two dimension"., https://doi.org/10.5281/zenodo.15341582, May 2025.

[24] Ślusarczyk Mateusz. https://github.com/Matusz1/mb_vortex, June 2025.

[25] Mateusz Ślusarczyk and Krzysztof Pawłowski. Vortices in the many-body excited states of interacting bosons in two dimensions. *Phys. Rev. A*, 111:053314, May 2025.

List of Figures

1.1 Abstract 11

2.1 Scheme showing energies of type I and type II excitations [2, 1] as functions of the momentum k. 16

2.2 Examples of a black soliton (black solid line) and a grey soliton (grey dashed line). The left panel shows the density profile, while the right panel displays the phase of the macroscopic orbital. A characteristic feature of solitons is the sharp phase variation at their center; in the case of the black soliton, this manifests as a phase jump of π, indicating a discontinuity. 17

2.3 Left: density n, and right: phase θ, of a quantized vortex in the mean-field orbital ϕ. In the core of the vortex the density drops to zero and the phase changes around that point by 2π. 18

3.1 Radial part $f_i(r)$ of the single particle wave function. For the angular momentum $m\hbar$ those are given by the m-th Bessel functions of the first kind, rescaled by consecutive zeros of the Bessel function, so that $f_i(R) = 0$. 21

4.1 Convergence of the ground state energy using exact diagonalization with the importance truncation scheme. The left panel shows the ground state energy as function of the inverse energy cutoff $1/E_{\mathrm{cut}}$ used to define the truncation search space $\mathcal{B}_{\mathrm{s}}$. The right panel displays the relative error of the ground state energy with respect to the lowest value, plotted as a function of E_{cut}. The results are shown for a system of $N = 6$ particles at the hightest considered interaction strength, $gN = 18\ \hbar^2/m$. The importance truncation parameters used are $\kappa_{\mathrm{min}} = 10^{-5}$ and $C_{\mathrm{min}} = 10^{-4}$. 31

5.1 Energy as a function of interaction strength for the yrast states with $L_z = 0$ (yellow solid line) and $L_z = N\hbar$ (blue solid line), compared with the mean-field energy (black dashed line) and the Bogoliubov–de Gennes correction (red dot-dashed line). The calculations were performed for $N = 6$ particles with a Gaussian width of $\sigma = 0.1R$. 36

5.2 Condensate fraction as a function of interaction strength for the yrast states with $L_z = 0$ (yellow solid line) and $L_z = N\hbar$ (blue solid line), along with the corresponding Bogoliubov–de Gennes prediction (red dot-dashed line). Calculations were performed for $N = 6$ particles with a Gaussian width $\sigma = 0.1R$. 37
5.3 Density profiles for several interaction strengths for the $L_z = 0$ yrast state, obtained from the single-particle density matrix (yellow solid lines) and the mean-field approximation (black dashed lines). Calculations were carried out for $N = 6$ particles with a Gaussian width $\sigma = 0.1R$. 37
5.4 Density profiles for several interaction strengths for the $L_z = N\hbar$ yrast state, shown using the single-particle density matrix (blue solid lines) and the mean-field approximation (black dashed lines). The calculations were performed for $N = 6$ particles with a Gaussian width $\sigma = 0.1R$. 38
5.5 Density of the mean-field orbital (black dashed line) shown alongside the densities $|v|^2$ of the two most highly occupied Bogoliubov–de Gennes modes. These two modes have approximately equal occupation and angular momenta $L_z = 0$ and $L_z = 2\hbar$, ensuring that the total angular momentum per particle remains at $N\hbar$. Calculations were performed for $N = 6$ particles, interaction strength $gN = 18\hbar^2/m$, and Gaussian width $\sigma = 0.1R$. 38
5.6 Density profiles for several interaction strengths for the $L_z = \frac{N}{2}\hbar$ yrast state, obtained from the single-particle density matrix (green solid lines) and the mean-field approximation (black dashed lines). Calculations were performed for $N = 6$ particles with a Gaussian width $\sigma = 0.1R$. 39
5.7 Conditional wave functions for $L_z = \frac{N}{2}\hbar$ (panel a) and $L_z = N\hbar$ (panel b). In each panel, the left column shows the density and the right column shows the phase of ψ_{cond}. When present, vortices appear off-center; this positional variation is more pronounced in panel (a). Calculations were performed for $N = 6$ particles, interaction strength $gN = 18\hbar^2/m$, and Gaussian width $\sigma = 0.1R$. 40

List of Tables

4.1 Size of the importance truncation search space $\mathcal{B}_s$ for increasing values of the energy cutoff E_{cut}. 30

Appendix A

Interaction integral

We derive the formula (3.24) for interaction integrals, we start from the general form

$$V_{ijkl} = \int \psi_i^*(\boldsymbol{r}_1)\psi_j^*(\boldsymbol{r}_2)V(|\boldsymbol{r}_1 - \boldsymbol{r}_2|)\psi_k(\boldsymbol{r}_1)\psi_l(\boldsymbol{r}_2)\,\mathrm{d}\boldsymbol{r}_1\,\mathrm{d}\boldsymbol{r}_2. \tag{A.1}$$

The single particle wave function ψ_j decomposed into radial and angular parts

$$\psi_j(\boldsymbol{r}) = f_j(r)e^{im_j\phi} \tag{A.2}$$

and the gaussian interaction potential

$$V(r) = \frac{g}{\sigma^2\pi}e^{r^2/\sigma^2} \tag{A.3}$$

could be inserted into (A.1). We use polar coordinates to write the distance between particles $|\boldsymbol{r}_1 - \boldsymbol{r}_2| = \sqrt{r_1^2 + r_2^2 - 2r_1r_2\cos(\phi_1 - \phi_2)}$ and to use as integration variables:

$$V_{ijkl} = \frac{g}{\sigma^2\pi}\int \mathrm{d}r_1\,\mathrm{d}r_2 r_1 r_2 f_i(r_1)f_j(r_2)f_k(r_1)f_l(r_2)e^{-\frac{r_1^2+r_2^2}{\sigma^2}} \tag{A.4}$$

$$\times \int \mathrm{d}\phi_1\,\mathrm{d}\phi_2 e^{i(-m_i\phi_1 - m_j\phi_2 + m_k\phi_1 + m_l\phi_2)}e^{\frac{2r_1r_2}{\sigma^2}\cos(\phi_1-\phi_2)}. \tag{A.5}$$

The two integrals over ϕ_1 and ϕ_2 could be solved by simple change of variables, keep ϕ_1 and defining $\phi = \phi_1 - \phi_2$ the integral (A.5) now becomes

$$\int_0^{2\pi}\mathrm{d}\phi_1 e^{i\phi_1(-m_i - m_j + m_k + m_l)}\int_0^{2\pi}\mathrm{d}\phi e^{i\phi(m_j - m_l)}e^{\frac{2r_1r_2}{\sigma^2}\cos\phi} = \tag{A.6}$$

$$= 2\pi\delta^{m_i+m_j}_{m_k+m_l}\int_0^{2\pi}\Big[\cos(\phi(m_j - m_l)) + i\sin(\phi(m_j - m_l))\Big]e^{\frac{2r_1r_2}{\sigma^2}\cos\phi} =$$

$$= 2\pi\delta^{m_i+m_j}_{m_k+m_l}\times 2\int_0^{\pi}\cos(\phi(m_j - m_l))e^{\frac{2r_1r_2}{\sigma^2}\cos\phi} =$$

$$= 4\pi^2\delta^{m_i+m_j}_{m_k+m_l}I_{|m_j-m_l|}\left(\frac{2r_1r_2}{\sigma^2}\right),$$

where we took advantage over the fact that imaginary part of the integral over ϕ vanishes and with the integral representation of the modified bessel function of the first kind

$$I_m(x) = \frac{1}{\pi}\int_0^{\pi} e^{x\cos\phi}\cos(n\phi)\,\mathrm{d}\phi. \tag{A.7}$$

The total interaction integral now takes the form of double integral over r_1 and r_2 from 0 to R and could be computed numerically

$$V_{ijkl} = \frac{4\pi g}{\sigma^2}\delta^{m_i+m_j}_{m_k+m_l}\int \mathrm{d}r_1\,\mathrm{d}r_2 r_1 r_2 f_i(r_1)f_j(r_2)f_k(r_1)f_l(r_2)e^{-\frac{r_1^2+r_2^2}{\sigma^2}}I_{|m_j-m_l|}\left(\frac{2r_1r_2}{\sigma^2}\right). \tag{A.8}$$